Progress In Electromagnetics Research, Vol. 132, 389–402, 2012

SOFT-FOCUSING IN ANISOTROPIC INDEFINITE MEDIA THROUGH HYPERBOLIC DISPERSION

S. Wheeland, A. V. Amirkhizi, and S. Nemat-Nasser*

Center of Excellence for Advanced Materials, Department of Mechanical and Aerospace Engineering, University of California, San Diego, La Jolla, CA, USA

Abstract—Materials that exhibit negative refraction may have many novel applications. We seek to evaluate the possibility of soft-focusing of microwave signals using a medium with an indefinite (hyperbolic) anisotropic permittivity tensor. We fabricated a 147 mm thick and 220 mm wide Styrofoam sample with an embedded array of 12-gauge brass wires of 6.35 mm lattice spacing. Two single-loop antennas were used to approximately generate a transverse magnetic (TM) point source and the associated detector. Using an Agilent 8510C Vector Network Analyzer (VNA), the frequency spectrum was scanned between 7 and 9 GHz. Relative gain or loss measurements were taken at equal spatial steps behind the sample. A scanning robot was used for automatic scanning in the x, y, and z directions, in order to establish the focusing patterns. The signal amplitudes measured in the presence and absence of the sample were compared. The robot was controlled using LabVIEW†, which also collected the data from the VNA and passed it to MATLAB‡ for processing. A soft focusing spot was observed when the antennas were placed in two different symmetric configurations with respect to the sample. These results suggest a method for focusing electromagnetic waves using negative refraction in indefinite (hyperbolic) anisotropic materials.

1. INTRODUCTION

There are many materials that exhibit an electrical plasmonic response. For these materials the electric permittivity is negative within certain frequency bands. However, few materials possess an

Received 2 August 2012, Accepted 24 September 2012, Scheduled 3 October 2012

* Corresponding author: Sia Nemat-Nasser (srmarsha@ucsd.edu).

† National Instruments Corporation™

‡ The MathWorks, Inc.®

equivalent magnetic response, i.e., negative magnetic permeability. Pendry et al. [1] and Smith et al. [2] theoretically and experimentally presented examples of microstructured materials with such magnetic properties. The combination of negative electrical permittivity and magnetic permeability was postulated by Veselago [3] to produce a negative index of refraction. The negative-index metamaterials and negative refraction were first established in 2000 [2]. This has stimulated considerable research activities ever since. One fascinating phenomenon observed in such media is the reversal of Snell's law. Pendry [4] presented an ideal design for a perfect lens with the index of refraction, n, equal to -1 and the characteristic impedance, Z, equal to the free space characteristic impedance, $+Z_0$. Even though such a design may be impractical, the general idea of using negative refraction to control a wave path has attracted considerable attention. Shen et al. [5] developed a compact lens in the visible spectrum using Pendry's theory. One notable example in the microwave regime was a flat, gradient lens, which showed focusing of close to +7 dB over incident power in the absence of the lens [6]. This demonstrates that negative-index materials could be used to focus microwave signals without the need for convex lenses.

The present work discusses a simple method for producing an anisotropic indefinite slab expected to produce similar soft-focusing. First, the theoretical prediction of soft-focusing in indefinite or hyperbolic media is explained. Next, the experimental work is discussed. We conclude by presenting results, which illustrate the focusing pattern in a variety of configurations.

2. THEORY

The majority of the microstructured metamaterials manufactured so far have been anisotropic. Smith et al. [7] noted that many interesting phenomena exist in cases where the diagonal components of the permittivity and permeability tensors have opposite signs. These materials are termed indefinite, since the permittivity tensor, $\boldsymbol{\varepsilon}$, (or the permeability tensor, $\boldsymbol{\mu}$) is neither positive- nor negative-definite. Consider a slab of such a material with transverse-magnetically polarized wave vectors that lie in an indefinite plane (i.e., the 12-plane for which the product of the corresponding permittivity tensor components, $\varepsilon_{11}\varepsilon_{22}$, is less than 0). When the group velocity is normal to the wave vector, the isofrequency curve is hyperbolic. An ellipse is seen in positive- or negative-definite media [8–14] (see Figure 1).

Such a shape of the isofrequency curve will result in negative refraction, a reversal of Snell's law, without the need for negative

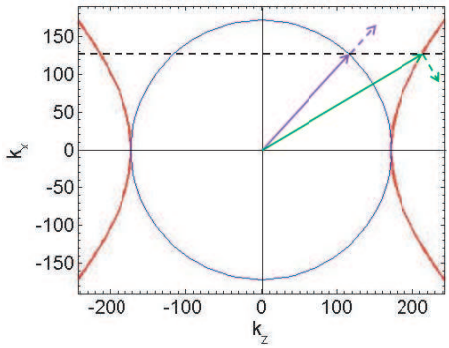

Figure 1. Isofrequency curves showing the distinction between free space (circle), where $\varepsilon_x > 0$ and $\varepsilon_z > 0$, and the indefinite medium presented in this paper (hyperbola), where $\varepsilon_x > 0$ and $\varepsilon_z < 0$. In both cases, z is in the direction of propagation. In indefinite media, waves are refracted negatively, as indicated by the green arrows. The solid vectors show the wave vector, while the dashed arrows show the group velocity direction. A similar calculation can be made when the magnetic permeability tensor is indefinite, as discussed in Smith et al. [14].

index. Consider the x-component of the group velocity and phase velocity vectors in (Figure 1). In a positive-definite medium, these components have the same sign while in an indefinite media they have the opposite sign. Smith et al. [14] illustrated this phenomenon with a ray-tracing diagram that was confirmed experimentally with split-ring resonators (SRR), which are magnetically indefinite media. In that study, the magnetic permeability along the axis of propagation was negative while all other diagonal components of the tensor were positive. Shallow incidence angles through the indefinite slab yielded similar focusing to that seen in the negative index slab. Liu et al. [9] and Fang et al. [10] demonstrated this numerically with finite element simulations. Focusing was seen with both ellipsoid and single-sheeted hyperboloid dispersion surfaces. Furthermore, Cheng and Ciu [11] developed a Luneburg microwave lens using the indefinite magnetic permittivity tensor produced in an array of I-shaped unit cells. Expanding upon these ideas, Salandrino and Engheta [12] also explored far-field scanless microscopy using metamaterial crystals. Simply put, hyperbolic dispersion in the indefinite slab results in partial focusing of a point source radiation on the opposite side of the slab [8–14] (see Figure 2).

For a square lattice array of simple elements with spacing d and

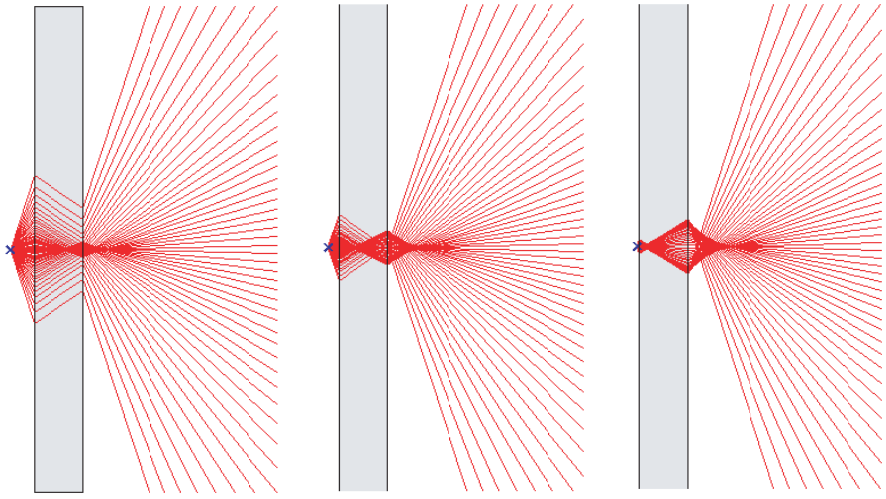

Figure 2. Indefinite slab showing partial focusing from a point source placed at a distance of (a) 7.35 cm, (b) 3.5 cm, and (c) 0.8 cm from the sample surface. This is an extension of the picture shown in Smith et al. [14]. In our work, a TM point source, rather than a TE one, is used. The Matlab program to create these images was kindly provided by Costas Soukoulis and Thomas Koschny from Iowa State University.

self-inductance L, the overall dielectric constant κ of the composite will have the following Drude-Lorentz form with k being the base material's dielectric constant [1, 15, 16]:

$$\kappa = \varepsilon_{\text{overall}}/\varepsilon_0 = k - \frac{f_p^2}{f^2} \tag{1}$$

where

$$f_p = \frac{\omega_p}{2\pi} \tag{2}$$

is the plasmon frequency,

$$\omega_p^2 = \frac{1}{d^2 L \varepsilon_0} \tag{3}$$

When the elements of the array are very thin straight wires of infinite length,

$$L = \frac{\mu_0}{4\pi}\left\{\ln\left[\frac{d^2}{\pi r^2}\right] - 1\right\} \tag{4}$$

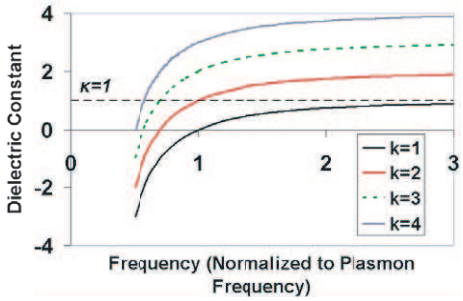

Figure 3. Graph of the relationship between dielectric constant and frequency for various values of k.

A graph showing the relationship between the frequency and κ is shown in (Figure 3) [18].

This permittivity form is valid only for an electric field polarized parallel to the wires. When the electric field is normal to the wires, the overall dielectric constant will be very close to that of the base composite, since the amount of metal is small. Therefore, if the wires are embedded in air and/or very low permittivity materials (such as Styrofoam), one may find a frequency at which $\varepsilon_{pw} = -\varepsilon_{nw} = -\varepsilon_0$. Here pw and nw denote polarizations parallel and normal to the wires, respectively. This frequency is simply:

$$f_{hyp} = f_p/2^{1/2} \tag{5}$$

We can extend the theoretical prediction by simulating a slab of such material in HFSS. Using Equations (1)–(4), the slab is homogenized and placed in an air box with radiation boundary conditions. Normal to the wires, $\kappa_{nw} = 1$ due to the very small volume fraction of metal embedded in the Styrofoam. A lumped port placed on a ring of copper provides the excitation for the system. This antenna mimics a point source. As shown in (Figure 4), the homogenized indefinite slab partially focuses the incident plane waves. In the figure, transmission is normalized with respect to measured values without the slab.

The plasmonic response can be further predicted using a parameter retrieval procedure similar to the one described in Nemat-Nasser et al. [17], though this is outside the scope of this paper. Previous work in this area indicates the expected plasmonic curve is similar to the theoretical prediction discussed here.

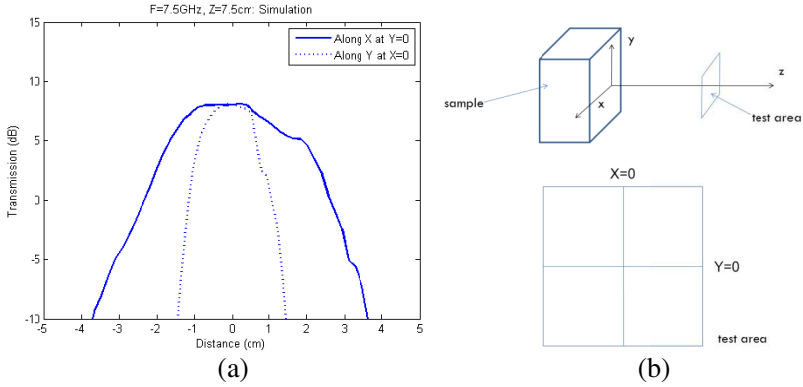

Figure 4. (a) Full-wave simulation of partially focused transmission through simulated homogeneous slab with $\varepsilon_x = \varepsilon_y = \varepsilon_0$ and $\varepsilon_z = -\varepsilon_0$ and (b) configuration schematics of the simulation.

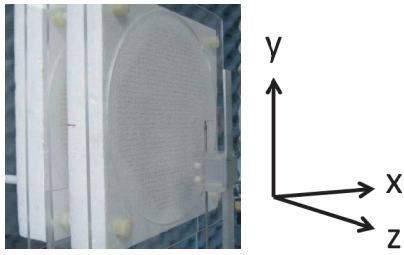

Figure 5. Styrofoam and 12-gauge brass wire sample secured with Plexiglas and threaded nylon rods.

3. METHODOLOGY

3.1. Sample

We constructed the sample for this series of experiments out of two rectangular Styrofoam blocks and 0.3065 mm diameter brass wires. The Styrofoam blocks each measured 50 mm thick and 350 mm wide, placed so the total thickness measured 147 mm; see (Figure 5). The wires were 147 mm long, arranged in an array with a lattice spacing of 6.35 mm. This was maintained by a series of holes in the Styrofoam blocks. Two square panels of Plexiglas with large circular holes were placed on either side of the Styrofoam for support. These were secured with threaded nylon rods, as shown in (Figure 5). Given this lattice geometry and using Equations (1)–(4), soft focusing was expected at

$f_{hyp} = 8.18\,\text{GHz}$.

3.2. Test Setup

To approximately create a TM point source and probe, two single-loop circular antennas with diameter 11 mm and wire thickness 0.29 mm were made. The antennas were arranged such that the linear coaxial feed was between the sample and the loop at all times, as shown in (Figure 6). This configuration was chosen during calibration since it resulted in cleaner measurements among all considered configurations. The stationary transmitter antenna was placed at a distance of 7.35 cm, 0.8 cm, or 3.5 cm from the center of the loop to the back surface of the sample. The receiver antenna scanned the space in the x, y, and z directions, starting from 4 cm, 2.3 cm, or 1.7 cm, respectively, from the front surface of the sample. The scanning was carried out by an XYZ automated scanning robot and controlled using LabVIEW. Each antenna was connected to the Agilent 8510C Vector Network Analyzer (VNA), where the signals originated and returned. At each point in the scanned space, the VNA measured the transmission component of the scattering matrix, S_{21}, for the requested frequency values. The data was then collected into a file on the controlling computer. (Figure 6) shows the test setup. In their magnetic counterpart study, Smith et al. [14] scanned a two-dimensional space with TE probes, using aluminum plates and absorbing material.

3.3. Calibration

The basic calibration of the experiment was done by running the robot without the sample in place to find the estimated transmission/power pattern due to the presence of the source. Even though the efficiency of the loop antenna TM source/probe is not ideal, we observed that in the spatial volume of interest the source increased the measured transmission coefficient from -75 dB to an average of -41 dB given a power input of 15 dBm. This power input value was used throughout the tests. Also, within the nominal $10 \times 10 \times 10$ cm box of measurement, the scanning setup was able to consistently stop at the same XYZ grid of $9.7 \times 9.5 \times 10.4$ cm.

3.4. Experimental Procedure

Each test was run with an averaging factor of 16 and 1% smoothing with an absolute power output of 15 dBm. In the x and y direction, the robot scanned either a 10×10 cm area over 201 or 401 frequency points

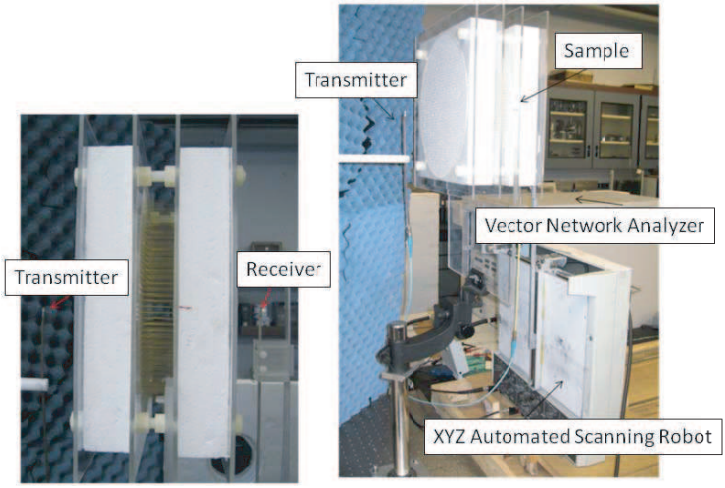

Figure 6. Test setup showing placement of two point source antennas around the sample with the robot and VNA — computer with LabVIEW not shown.

or a 20×20 cm area over 401 frequency points within a range of 7–9 GHz. This provided a detailed set of data. The tests were carried out with and without the sample in place. The VNA sent the signals to the transmitter antenna. Using a LabVIEW module, the VNA-measured signal from the receiver antenna was collected in a file readable by MATLAB. In other words, the data sent to MATLAB represents S_{21}, where ports 1 and 2 represent the transmitter and receiver antennas, respectively. This procedure was repeated at each stop of the receiver probe.

4. RESULTS

Three sets of tests are presented in this section, corresponding to the three transmitting antenna locations mentioned previously. The results shown in (Figure 7) and (Figure 8) are obtained when the center of the transmitter loop is placed 7.35 cm from the back surface of the sample. (Figures 9) and (Figure 10) show the experimental results when this distance is changed to 0.8 cm and 3.5 cm, respectively.

As can be seen from the first set of tests in (Figure 7), the strongest focusing occurs at 7.6 GHz at a distance of 7.5 cm from the sample surface. A distinction can be made between the data with the sample and without the sample. It should be noted that the signals focused at

a lower frequency than the theoretically predicted 8.18 GHz. A possible explanation for this discrepancy is discussed in the next section.

Illustrated in (Figure 8(a)), the strongest focusing is seen at 7.5 cm from the front surface of the sample. This is consistent with the predicted focal distance, which is based on the distance between the transmitter antenna and the back surface of the sample.

The second set of tests with the transmitter antenna at a distance of 0.8 cm from the back surface show similar results, as can be seen in (Figure 9). The focal point in this case is very close to the front surface of the sample, as expected from a ray tracing analysis of this configuration.

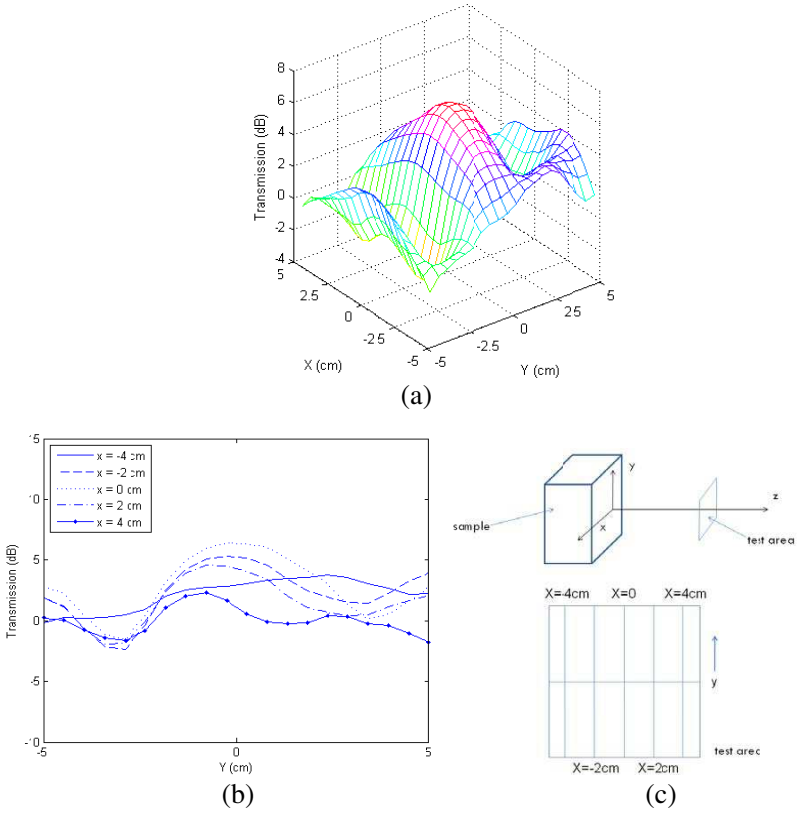

Figure 7. Transmitter antenna at 7.35 cm distance. (a) Power gain compared to the measurement without the sample as a function of X and Y at $Z = 7.5$ cm (from sample surface) and $F = 7.6$ GHz; (b) power gain as a function of Y at $Z = 7.5$ cm and $F = 7.6$ GHz at various values of X; (c) schematics of the test configuration.

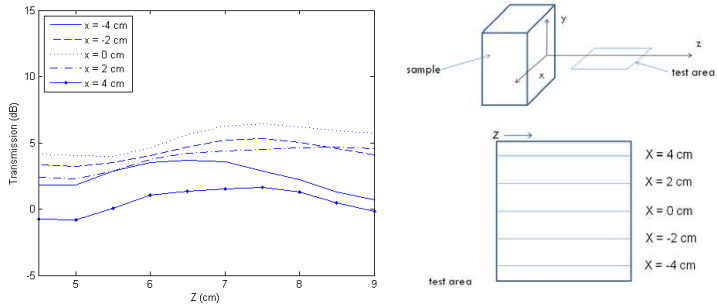

(a) (b)

Figure 8. Transmitter antenna at 7.35 cm distance. (a) Power gain compared to the measurement without the sample as a function of Z for various values of X at $F = 7.6$ GHz and $Y = 0$ cm; (b) schematics of the test configuration.

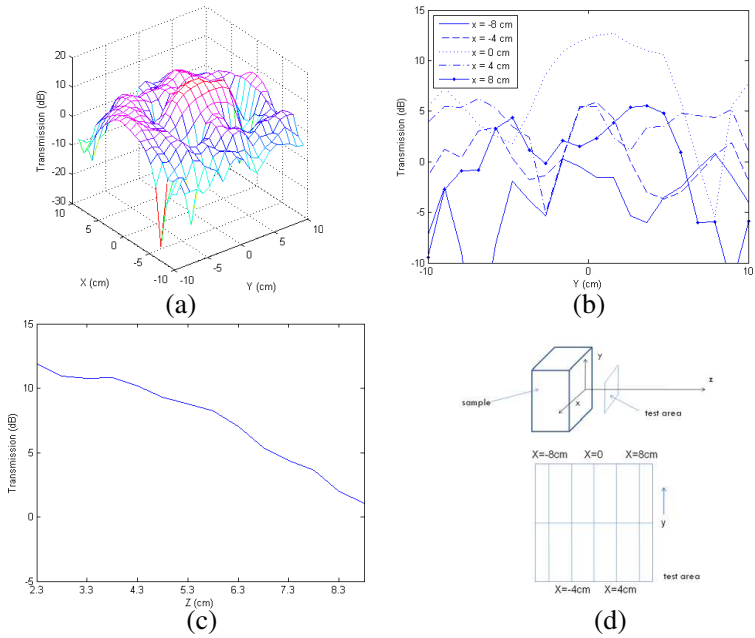

(a) (b) (c) (d)

Figure 9. Transmitter antenna at 0.8 cm distance. (a) Power gain compared to the measurement without the sample as a function of X and Y at $Z = 2.3$ cm (from sample surface) and $F = 7.6$ GHz; (b) power gain as a function of Y at $Z = 2.3$ cm and $F = 7.6$ GHz at various values of X; (c) power gain at the center of the sample over the z-axis; (d) schematics of the test configuration.

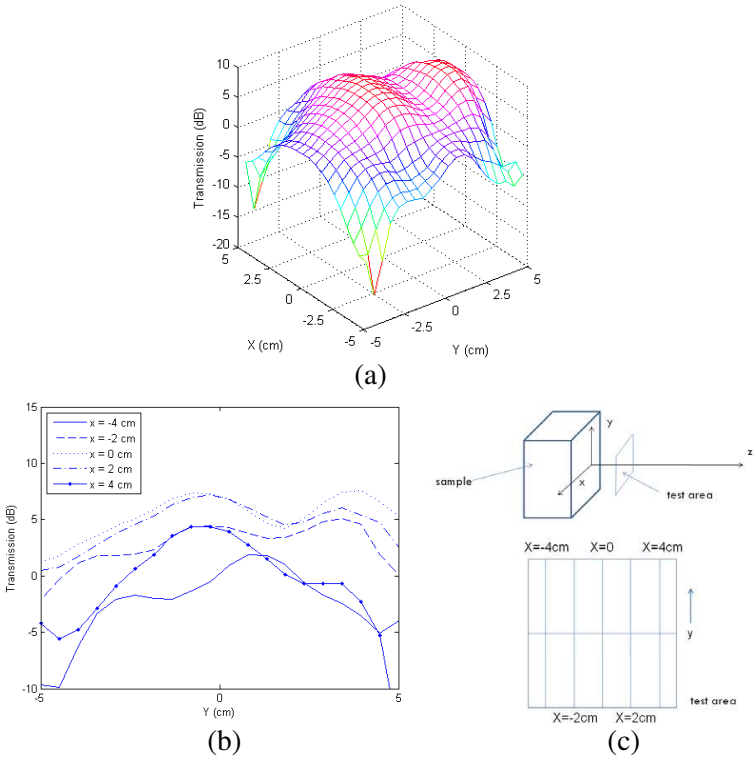

Figure 10. Transmitter antenna at 3.5 cm distance. (a) Power gain compared to the measurement without the sample as a function of X and Y at $Z = 3.7$ cm (from sample surface) and $F = 7.6$ GHz; (b) power gain as a function of Y at $Z = 3.7$ cm and $F = 7.6$ GHz at various values of X; (c) schematics of the test configuration.

A final set of tests with the transmitter antenna at a distance of 3.5 cm from the back surface of the sample show similar results as well, see (Figure 10). Notice the slight focusing towards the center of the sample and towards the top.

5. CONCLUSIONS

In the earlier study with the SRR lattice, Smith et al. [14] found that an imperfect focal spot is achieved with $\mu_y < 0$, $\mu_x > 0$. The results of the experiments presented here show that the sample decreases the amount of signal loss at predicted soft-focus spots compared to that without the sample in place. Though this difference is small, the

sample focuses at a 7.5 cm distance from the front surface in the 7.35 cm test at a frequency of 7.6 GHz with softer focusing at other frequencies and distances. This frequency is lower than the calculated value of 8.18 GHz. Equations (1)–(4) assume an infinitely long wire, whereas finite lengths of wire were used in the sample. The effect of finite length of the wires on the mobility of electrons is most pronounced at the interface between the wire array and the air. It is possible that within a distance inside the wire array comparable to the wavelength of interest, the overall dielectric constant may not be estimated by Equations (1)–(4). This is due to the strong capacitive effect of the ends of the wires. A theoretical model for this may be possible to derive, but it is outside the scope of this experimental paper. However, full-wave simulations agree with the results of the experiment. Better antenna construction could allow for higher transmission coefficients. Also, enclosing the whole system in an anechoic chamber would reduce ambient reflection and could improve signal reception. In summary, these results demonstrate hyperbolic focusing within media with an indefinite dielectric constant tensor.

ACKNOWLEDGMENT

The authors would like to thank Costas Soukoulis and Thomas Koschny from Iowa State University for the MATLAB program used to create the second figure. This research has been conducted at the Center of Excellence for Advanced Materials (CEAM) at the University of California, San Diego with partial support from AFOSR/MURI Grant FA9550-06-1-0337 to Kent State University, subaward 444286-PO61719 to University of California, San Diego.

REFERENCES

1. Pendry, J. B., A. J. Holden, W. J. Stewart, and I. Youngs, "Extremely low frequency plasmons in metallic mesostructures," *Physical Review Letters*, Vol. 76, No. 25, 4773-6, 1996.
2. Smith, D. R., W. J. Padilla, D. C. Vier, S. C. Nemat-Nasser, and S. Schultz, "A composite medium with simultaneously negative permeability and permittivity," *Physical Review Letters*, Vol. 84, 4184-7, 2000.
3. Veselago, V. G., "The electrodynamics of substances with simultaneously negative values of ε and μ," *Soviet Physics USPEKHI*, Vol. 10, No. 4, 509, 1968.

4. Pendry, J. B., "Negative refraction makes a perfect lens," *Physical Review Letters*, Vol. 85, No. 18, 3966-9, 2000.
5. Shen, N. H., S. Foteinopoulou, M. Kafesaki, T. Koschny, E. Ozbay, E. N. Economou, and C. M. Soukoulis, "Compact planar far-field superlens based on anisotropic left-handed metamaterials," *Physical Review Letters B*, Vol. 80, 115123, 2009.
6. Driscoll, T., D. N. Basov, A. F. Starr, P. M. Rye, S. Nemat-Nasser, D. Schurig, and D. R. Smith, "Free-space microwave focusing by a negative-index gradient lens," *Applied Physics Letters*, Vol. 88, 081101-1–3, 2006.
7. Smith, D. R. and D. Schurig, "Electromagnetic wave propagation in media with indefinite permittivity and permeability tensors," *Physical Review Letters*, Vol. 90, No. 7, 077405-1–4, 2003.
8. Smith, D. R., P. Kolinko, and D. Schurig, "Negative refraction in indefinite media," *Journal of the Optical Society of America B: Optical Physics*, Vol. 21, No. 5, 1032-42, 2004.
9. Liu, H., Q. Lv, H. Luo, S. Wen, W. Shu, and D. Fan, "Focusing of vectorial fields by a slab of indefinite media," *Journal of Optics A: Pure and Applied Optics*, Vol. 11, 105103, 2009.
10. Fang, A., T. Koschny, and C. M. Soukoulis, "Optical anisotropic metamaterials: Negative refraction and focusing," *Physical Review Letters B*, Vol. 79, 245127, 2009.
11. Cheng, Q. and T. J. Cui, "Planar microwave lens based on complementary metamaterials," *2010 IEEE Antennas and Propagation Society International Symposium (APSURSI)*, 1–4, 2010.
12. Salandrino, A. and N. Engheta, "Far-field subdiffraction optical microscopy using metamaterial crystals: Theory and simulations," *Physical Review Letters B*, Vol. 74, 075103, 2006.
13. Schurig, D. and D. R. Smith, "Spatial filtering using media with indefinite permittivity and permeability tensors," *Applied Physics Letters*, Vol. 82, No. 14, 2215-7, 2003.
14. Smith, D. R., D. Schurig, J. J. Mock, P. Kolinko, and P. Rye, "Partial focusing of radiation by a slab of indefinite media," *Applied Physics Letters*, Vol. 84, No. 13, 2244-6, 2004.
15. Nemat-Nasser, S. C., A. V. Amirkhizi, W. J. Padilla, D. N. Basov, S. Nemat-Nasser, D. Bruzewicz, and G. Whitesides, "Terahertz plasmonic composites," *Physical Review E*, Vol. 75, 036614-1–7, 2007.
16. Smith, D. R., D. C. Vier, W. J. Padilla, S. C. Nemat-Nasser, and S. Schultz, "Loop-wire medium for investigating plasmons at

microwave frequencies," *Applied Physics Letters*, Vol. 75, No. 10, 1425-7, 1999.

17. Nemat-Nasser, S., S. C. Nemat-Nasser, T. Plaisted, A. Starr, and A. V. Amirkhizi, "Multifunctional materials," *BIOMIMETICS: Biologically Inspired Technologies*, Y. Bar-Cohen, Ed., 309–341, CRC Press, 2005.
18. Marshall, S., A. V. Amirkhizi, and S. Nemat-Nasser, "Focusing and negative refraction in anisotropic indefinite permittivity media," *Proceedings of the International Society for Optical Engineering Electroactive Polymer Actuators and Devices (EAPAD)*, Y. Bar-Cohen, T. Wallmersperger (eds.), San Diego, 2009.